

THE DECLINE OF THE SOURCE POPULATION OF GAMMA-RAY BURSTS AND THEIR LUMINOSITY FUNCTION

B. E. STERN^{1,2,3}, YA. TIKHOMIROVA^{2,3}, R. SVENSSON³
Draft version November 18, 2018

ABSTRACT

The source population of gamma-ray bursts (GRBs) declines towards the present epoch being consistent with the measured decline of the star formation rate. We show this using the brightness distribution of 3255 long BATSE GRBs found in an off-line scan of the BATSE continuous 1.024 s count rate records. The significance of this conclusion is enhanced by the detection of three GRBs with known redshifts brighter than 10^{52} erg s⁻¹ during the last two years. This is an argument in favor of the generally believed idea that GRBs are strongly correlated with the star production, at least on cosmological time scales, and favors the association of long GRBs with collapses of supermassive stars. However, we still cannot rule out neutron star mergers if the typical delay time for binary system evolution is relatively short. If we assume a steep decline of the GRB population at $z > 1.5$, then their luminosity function can be clearly outlined. The luminosity function is close to a power law, $dN/dL \propto L^{-1.4}$, for low luminosities over at least 1.7 orders of magnitude. Then the luminosity function breaks to a steeper slope or to an exponential decline around $L \sim 3 \cdot 10^{51}$ erg s⁻¹ in the 50 - 300 keV range assuming isotropic emission.

Subject headings: gamma-rays: bursts – methods: data analysis

1. INTRODUCTION

In spite of the remarkable progress that has proved the cosmological origin of GRBs, there remains a number of extremely important issues which are still not resolved. Some of the main issues dealt with in this work are the following. (i) What is the cosmological evolution of the source population of gamma-ray bursts (GRBs)? Does it evolve as the star formation rate (hereafter the SF rate) or does it has its own specific evolution? (ii) What is the luminosity distribution (or function) of GRBs? (iii) What is the total rate of GRBs in the universe?

There are two competing approaches for such studies: (i) the “statistical” one using large samples of poorly localized GRBs, and (ii) the “individual” one, using the small sample of optically followed-up GRBs, where we have additional information per event including the redshift and the intrinsic luminosity.

The main data array for statistical studies was supplied by the Burst And Transient Source Experiment (BATSE) (Fishman et al. 1989) onboard the *Compton Gamma-Ray Observatory (CGRO)*. The BATSE sample⁴ is a few times larger than the yield of all other experiments that have detected GRBs. It includes 2702 events in its final form.

Fitting the BATSE data to various cosmological/evolutionary models has been the subject of many studies since the start of the BATSE operation in 1991. For references to early works on fitting the BATSE brightness distribution of GRBs to cosmological models, see Bulik (1999). For a number of results setting an upper limit to the width of the luminosity function of GRBs, see, e.g., Hakkila et al. (1996). Then Loredo & Wasserman (1998) demonstrated that the 3rd BATSE catalog does not constrain the luminosity function. Later work using the larger sample of the 4th BATSE catalog gave few constraints. Krumholtz, Thorsett, & Harrison (1998) fitting the BATSE sample at peak fluxes $P > 0.42$ photons s⁻¹ cm⁻² found that both a non-evolving GRB source population and SF evo-

lutionary models fit the data even using standard candle GRBs. Wijers et al. (1998) demonstrated the same for the SF model. Totani (1999) showed that the SF model does not fit the data using the standard candle assumption. Panchenko (1999) using the SF model accounting for the time delay due to binary system evolution estimated the minimal width of the luminosity function as being two orders of magnitude in luminosity. Finally, the recent work of Porciani & Madau (2001) deals with a larger sample including the BATSE non-triggered bursts of Kromers et al. (2000) extending the peak flux down to 0.18 photons s⁻¹ cm⁻². They found that the data fit cannot distinguish between different variants of the GRB source evolution at large redshifts. However, they did not check how sensitive the fit is to the evolution at *low* redshifts.

The general impression arising from fitting the BATSE data using cosmological models was that this approach had little future. Indeed, the “statistical” approach demonstrated an agreement between the data and a wide set of models. The very few constraints obtained were trivial.

The main reason for the poor progress so far is the insufficient depth of the BATSE sample, i.e., the too narrow brightness range. The brightest burst has a peak photon flux of 160 photons s⁻¹ cm⁻². Bursts useful for a usual least χ^2 fit are, however, at $P < 30$ photons s⁻¹ cm⁻². The BATSE trigger threshold is at 0.2 photons s⁻¹ cm⁻² but the bursts near the threshold are difficult to use because of poorly known threshold effects. All works cited above used the peak flux range above 0.4 or even above 1 photon s⁻¹ cm⁻², which is then narrower than two orders of magnitude. Loredo and Wasserman (1998) showed that this is a too narrow range for obtaining constraints from the fits.

The “individual” approach gave a wealth of important data. By itself this approach is, however, still unable to resolve the issues stated above. Besides having a too poor statistics (presently we have only 17 GRBs with known redshifts), the

¹ Institute for Nuclear Research, Russian Academy of Sciences, Moscow 117312, Russia

² Astro Space Center of Lebedev Physical Institute, Moscow, Profsoyuznaya 84/32, 117810, Russia

³ SCFAB, Stockholm Observatory, SE-106 91 Stockholm, Sweden

⁴ The catalog is available at <http://gamma-ray.msfc.nasa.gov/batse/grb/catalog/current/>

approach is subjected to very strong selection biases. Nevertheless, this small sample tells us that the luminosity function is at least 2.5 orders of magnitude wide and that it extends up to $\sim 3 \cdot 10^{52}$ erg s $^{-1}$.

After most previous work in this area was completed, the following progress concerning the data accumulation has taken place:

- BATSE obtained additional data until the deorbiting of *CGRO* in June 2000.

- Searches for non-triggered bursts were performed by Schmidt (1999), Kommers et al. (2000), and Stern et al. (2000, 2001). In the latter work, the statistics of useful GRB events was increased by a factor 1.7 and the threshold effect was measured. Thus, the useful fitting range was extended down to 0.1 photons s $^{-1}$ cm $^{-2}$.

- A sample of GRBs with known intrinsic luminosities (presently 17 events) appeared due to the optical afterglow observations.

In this work, we use these advances including the “individual” GRB data. In addition, we include the brightest peak flux interval, which is statistically poor, into the maximum likelihood fit and find that this peak flux interval is very informative. Thus we extend the fitting brightness range to 3 orders of magnitude. This allow us to obtain a number of conclusive results.

In §§2-4, we describe the set of fitted data, the fitting models including the cosmology, the source evolution, and the luminosity function of GRBs, and finally the the fitting procedure. In §5, we present results of the fits and show that the scenario of a non-evolving population of GRBs does not fit the data. Instead, we demonstrate that the GRB-population should decline approximately as fast as the star formation rate. We also determine the approximate shape of the luminosity function and give an estimate for the lower limit of the total rate of GRBs as being 3000 GRBs per year in the visible universe (that is up to a reasonably large redshift).

2. THE DATA

Probing various cosmological and evolutionary models we fitted the sample of 3255 BATSE GRBs longer than 1 s found by Stern et al. (2000, 2001) in the off-line scan of the BATSE continuous daily records in 1.024 s time resolution. This sample, which is selected from the catalog of Stern & Tikhomirova⁶, is essentially uniform and has a corresponding efficiency matrix (measured by a test burst method), which is needed when fitting the weak end of the log N - log P distribution. (Hereafter the term log N - log P distribution means the *differential* distribution of GRBs vs. the logarithm of the *peak photon flux*). We excluded short bursts (consisting of one 1.024 s bin) from the analysis for two reasons: (i) short and long bursts could be separate phenomena, and (ii) the sample is incomplete regarding short bursts as they have a lower detection efficiency and a wrong brightness estimate in 1.024 s time resolution. By excluding one-bin events, we make our sample more homogeneous.

The brightness distribution of the GRBs in this sample was fitted using a hypothetical brightness distribution folded with the detection efficiency matrix described in Stern et al. (2001). This matrix was obtained using a sample of $\sim 11,000$ artificial

⁶ see http://www.astro.su.se/groups/head/grb_archive.html

⁷ see, e.g., <http://www.aip.de/jcg/grb.html>

⁸ see <http://www.asdc.asi.it/bepposax/>

⁹ <http://ssl.berkeley.edu/ipn3/index.html>

test bursts, which were superimposed on the BATSE continuous records and then passed through the same procedure of search and processing as real GRBs. The efficiency matrix is approximately given by

$$F(c_e, c_m) = E(c_e) \frac{1}{\sigma \sqrt{\pi}} \exp \left[-\frac{\log^2(c_m/c_{mo})}{2\sigma^2} \right], \quad (1)$$

where c_e is the expected and c_m the measured count rate in units of counts s $^{-1}$ cm $^{-2}$; $E(c_e) = 0.70(1 - \exp[-(c_e/c_{eo})^2])^\nu$ is the efficiency function with fitted parameters $c_{eo} = 0.097$ counts s $^{-1}$ cm $^{-2}$, $\nu = 2.34$; the log-normal factor describes the relative error of the measured count rate, $\sigma = 0.09(0.08/c_e)^{1/2}$, and the selection bias is crudely expressed as $c_{mo} = c_e + 0.05 \exp(-c_e/0.05)$.

In order to constrain the intrinsic luminosity function (hereafter the luminosity function or the LF), we used the sample of gamma-ray bursts with measured redshifts⁷. We cannot infer the LF from this sample as it is subjected to strong selection biases. This is demonstrated in section 3.3. The redshift data, however, give us a useful piece of information, i.e., the existence of very intrinsically bright GRBs. Three of the intrinsically brightest bursts are: GRB990123, GRB991216, and GRB000131 (named by dates), with redshifts 1.6 (Djorgovski et al. 1999), 1.02 (Vreeswijk et al. 1999), and 4.5 (Andersen et al. 2000), respectively, and with BATSE peak fluxes 16.4, 67.5, and 6.3 photons s $^{-1}$ cm $^{-2}$ in the 50 - 300 keV range, respectively (estimated using the BATSE catalog). If they were emitted at $z = 1$, their peak fluxes taking into account the “K-correction” (i.e., the correction due to the spectral redshift effects on a fixed spectral band of the detector) would be 45, 69, and 84 photons s $^{-1}$ cm $^{-2}$, respectively, assuming the cosmological parameters $(\Omega_M, \Omega_\Lambda) = (1, 0)$. Hereafter, we use the photon peak flux at redshift $z=1$, I , as a measure of the intrinsic brightness. We, furthermore, use the intrinsic brightness interval of these three events, $I > 40$ photons s $^{-1}$ cm $^{-2}$, to constrain the LF when fitting the BATSE log N - log P distribution. The choice of the three brightest events for this purpose is somewhat arbitrary. We cannot use a much wider brightness interval because of a brightness dependent selection bias. On the other hand, we can neglect such problems for the narrow brightness range of these three events. The data we fitted are presented in Figure 1.

In order to impose a proper constraint on the LF we must estimate the sampling function for strong GRBs. With the sampling function we mean the probability that a burst will be detected, localized, its afterglow observed and its redshift measured. This function evolves with time. It was zero before 1997. Then this function was limited by the field-of-view of the two Beppo-Sax Wide Field Cameras, ~ 0.08 of the sky⁸, as this was the main instrument supplying precise coordinates of GRBs during 1997 - 1998.

In 1999 and 2000, many precise localizations were made by other systems, with most of them being made by the interplanetary network *Ulysses/Konus/Near* (see the IPN home page⁹). This means that in this period the sampling function became larger and for very bright events it could, in principle, approach unity as all instruments of the IPN had a 4π field-of-view. Actually it should be considerably less as in the same period, three very strong BATSE events (triggers 7301, 7491,

7595) were not localized. For one strong BATSE event (trigger 7954, GRB000115) an X-ray transient was found, but no optical transient. With this background, let us take a conservatively high estimate of the sampling function, $S_{40} = 0.5$ for GRBs with $I > 40$ photons $\text{s}^{-1} \text{cm}^{-2}$, and the conservatively low estimate of the rate of these GRBs, $N_{40} = 3 \text{ yr}^{-1}$, in the visible universe.

3. FITTING MODELS

3.1. Cosmology

We tried two sets of cosmological parameters, the flat matter-dominated universe, commonly used in most of previous works: $(\Omega_M, \Omega_\Lambda) = (1, 0)$ and the vacuum-dominated cosmology, which is supported by recent data $(\Omega_M, \Omega_\Lambda) = (0.3, 0.7)$ (see, e.g., Lukash, 2000). Hereafter, these two models are denoted as M-models and Λ -models, respectively. The distribution of GRBs over redshift for a non-evolving (NE) population for $\Omega_M + \Omega_\Lambda = 1$ is

$$\frac{dN}{dz} \propto \frac{1}{1+z} \frac{1}{\sqrt{\Omega_\Lambda + \Omega_M(1+z)^3}} \left(\int_0^z \frac{dz'}{\sqrt{\Omega_\Lambda + \Omega_M(1+z')^3}} \right)^2 \quad (2)$$

The photon number “luminosity” distance is defined by

$$d_L = \frac{c}{H_0} \sqrt{1+z} \int_0^z \frac{dz'}{\sqrt{\Omega_\Lambda + \Omega_M(1+z')^3}}, \quad (3)$$

where H_0 is the Hubble constant, which is assumed to be $75 \text{ km s}^{-1} \text{Mpc}^{-1}$, when estimating the luminosities of GRBs. For the standard luminosity distance, the factor $\sqrt{1+z}$ is replaced with $1+z$.

3.2. Evolution of the Source Population

Another important component of the model is the evolution of the population of GRB sources. We probed four cases: a non-evolving population and three evolution functions correlated with the history of star formation following Porciani & Madau (2001). The declining phase of the star formation (SF) rate at $z < 1.5$ is a relatively well measured function of z . Its history at $z > 2$ is, however, controversial. This issue is discussed in Porciani & Madau (2001) giving the relevant references. Below we reproduce three versions of the SF evolution suggested in that work:

$$R_{\text{SF1}}(z) = \frac{0.3e^{3.4z}}{(e^{3.8z} + 45)} \quad \text{M}_\odot \text{ yr}^{-1} \text{Mpc}^{-3}, \quad (4)$$

i.e., decreasing SF at $z > 1.5$,

$$R_{\text{SF2}}(z) = \frac{0.15e^{3.4z}}{(e^{3.4z} + 22)} \quad \text{M}_\odot \text{ yr}^{-1} \text{Mpc}^{-3}, \quad (5)$$

i.e., roughly constant SF at $z > 2$,

$$R_{\text{SF3}}(z) = \frac{0.134e^{3.05z}}{(e^{2.93z} + 15)} \quad \text{M}_\odot \text{ yr}^{-1} \text{Mpc}^{-3}, \quad (6)$$

i.e., increasing SF at large z .

Models will from now on be denoted as NE,M; SF1, Λ ; and so on, where M and Λ denotes the two types of cosmologies.

The next step is the generation of the standard candle $\log N - \log P$ distributions. At this step, we introduced an additional broadening of the observed brightness distribution due to the

K-correction which depends on the type of GRB spectrum. For this purpose, we obtained the $\log N - \log P$ distributions using Monte-Carlo simulations. To each simulated GRB we prescribed one of 54 spectra of bright BATSE bursts parametrized by the Band expression (Band et al. 1993). All these template spectra were assumed to be emitted at $z=1$. Then we sampled the z of the burst and the corresponding K-correction for the 50 - 300 keV band was applied to the apparent brightness of the simulated GRB.

The resulting $\log N - \log P$ distributions are shown in Figure 2. If we neglect the K-correction which depends on the GRB spectrum, then each distribution in Figure 2 is a direct reflection of the corresponding redshift distributions of GRBs. The standard candle luminosity (before applying the K-correction) corresponds to a peak photon flux of 1 photon $\text{s}^{-1} \text{cm}^{-2}$ in the 50 - 300 keV band at $z=1$.

If we vary this value when fitting the data, none of the 8 models (two cosmological cases, four evolutionary cases) would still fit the observed $\log N - \log P$ distribution of 3255 long BATSE GRBs (shown by the crosses in Figure 2). The fact that the evolution of the SF1 type with the standard candle luminosity function cannot fit data was shown by Totani (1999) and Lloyd & Petrosian (1999). The NE model gives the smallest deviation in this case, but still the value of χ^2 is unacceptable (61 for 27 degrees of freedom). However, as it will be shown below, the discrepancy in the case of the NE model can not be compensated by any hypothesis of the luminosity function.

The slopes of the three $\log N - \log P$ distributions for an evolving SF rate are close to the Euclidean slope $-3/2$ starting from a peak flux $P \sim 1$ photon $\text{s}^{-1} \text{cm}^{-2}$, which at this standard candle brightness corresponds to $z=1$. The agreement with the Euclidean slope is an accidental coincidence due to the superposition of cosmological and evolutionary effects.

3.3. Parametrization of the Luminosity Function

As was stated above, the luminosity distribution of events with known z cannot be used as a base for the LF model in the whole brightness range. This fact is clear from Figure 3 where we present $\log N - \log P$ distributions that would give the sample of 17 GRBs with known absolute luminosities for the NE, SF2 and SF3 evolutionary models. All models give a striking disagreement with the data. The only way to reduce this disagreement is to assume an unreasonably sharp increase of GRBs at large redshifts which, in turn, will contradict the redshift data. Therefore the shape of a hypothetical LF remains arbitrary (except the constraints imposed on the brightest end of the LF).

In order to get a handle on the LF of GRBs, we tried different types of functions that describe common shapes of wide distributions in nature: the log-normal distribution (LGN), a truncated power law (TPL), a power law with an exponential cutoff (PLexp), and a broken power law (BPL).

LGN: $dN/dI = C \cdot \exp(-(\ln^2(I/I_0)/2\delta^2))$, with three free parameters I_0 , δ , and C .

TPL: $dN/dI = C \cdot I^{\alpha-1}$ for $I_1 < I < I_0$ and 0 outside this interval. Free parameters are α , I_1 , I_0 , and C . In some fits, I_1 was fixed to $-\infty$ leaving 3 free parameters.

PLexp: $dN/dI = C \cdot I^{\alpha-1} \cdot \exp(-I/I_0)$, with three free parameters α , I_0 , and C .

BPL: $dN/dI = C \cdot I^{\alpha-1}$ for $I_1 < I < I_0$, $dN/dI = C_1 \cdot I^{\alpha+\beta-1}$ for $I_0 < I < I_2$ and $dN/dI = 0$ outside the $[I_1, I_2]$ interval. Free parameters are α , β , I_1 , I_0 , and C , while I_2 was fixed to a value

above the maximum observed GRB brightness.

We also considered a smoothed version of the broken power law:

$$\text{SBPL: } dN/dI = CI^{\alpha-1}/(1 + (I_0/I)^\beta)$$

For technical convenience, we measure the intrinsic brightness as peak count rate or peak photon flux, I , in the 50 - 300 keV range produced by a GRB at a distance corresponding to $z = 1$. The absolute peak luminosity of the GRBs is related to I as $L = I \cdot 3 \cdot 10^{50} \text{ erg s}^{-1}$ assuming isotropic emission. Below we present the main results on the LF both in I and in absolute luminosity units.

4. THE FITTING PROCEDURE

We used the forward folding method when fitting the observed distribution of GRBs, i.e., the hypothetical brightness distribution was convolved with the efficiency matrix (1) and fitted to the observed distribution of GRBs over peak count rate (crosses in Figure 2). This distribution was represented by 29 data points spaced by 0.1 in $\log P$ in the interval 0.067 - 50 photons $\text{s}^{-1} \text{cm}^{-2}$ in the 50 - 300 keV range. During 9.1 years, there are 3 GRBs detected by BATSE that are brighter (the rightmost cross in Figure 2 and one GRB at 160 photons $\text{s}^{-1} \text{cm}^{-2}$, which is not shown). We treat this brightness range separately, estimating the likelihood function of the fit for each peak flux interval. For the main interval, this is the standard χ^2 probability function. For the tail of the brightness distribution, the likelihood is the Poisson probability to sample not more than 3 events brighter than 50 photons $\text{s}^{-1} \text{cm}^{-2}$ at the given number of such events for the full observation period, M_{50} , predicted by the model. The final likelihood function is the product of these two factors.

Instead of the usual χ^2 minimization procedure, we explore the parameter space sampling $\sim 10^5$ random points. This is sufficient to find the minimum of χ^2 with a good accuracy while at the same time investigating the χ^2 “topography” of the parameter space region. This method does not work if the “valley” of the minimum has a very small volume in parameter space. For our cases, the minima are wide and smooth enough.

The maximum likelihood point for the whole sample of points in parameter space represents the *unconstrained* fit, where the requirement of the redshift data, $N_{40} > 3 \text{ yr}^{-1}$, was ignored. The subsample selected including this requirement represents the *constrained* fit. The effective number of degrees of freedom (DOF) in the second case is smaller by unity as compared to the unconstrained fit. We present results of both the constrained and the unconstrained fits in order to demonstrate the role of the redshift data and the possible effects of the uncertainty in the estimate of the rate of intrinsically strong GRBs.

The best fit parameters are presented in Tables 1 and 2. Table 1 includes fits using various LF models and selected cosmological models. Table 2 summarizes fits using a broken power law LF for all cosmological models and provides data to compare their relevance using a Bayesian approach.

5. RESULTS

5.1. Rejection of models without source evolution

The best unconstrained fit using the NE models has $\chi^2 = 36.8$ for 25 degrees of freedom (Table 1, truncated power law, TPL), which is marginally acceptable if we ignore the tail of the brightness distribution. For the tail, the model predicts M_{50}

$= 11.5$, while the real number is 3 yr^{-1} and the corresponding maximum likelihood drops down to $1.3 \cdot 10^{-4}$ (see Table 1). When we impose the redshift data constraint, $N_{40} > 3 \text{ yr}^{-1}$, the maximum likelihood factor that we can obtain using the NE,Λ model is $3.2 \cdot 10^{-6}$, which is for the case of a broken power law LF (see Table 2). For the NE,M model, the results are even worse.

The likelihood factor is not yet a rejection factor for the NE model, because we cannot exclude some bias or contamination which would increase the χ^2 . To reject the NE hypothesis, we should demonstrate a good fit for other equally simple and reasonable models. Indeed, data fits with the SF models are much better (see Tables 1 and 2). Their maximum likelihood factor is about 0.02. This is the case when we can apply the Bayesian approach. The estimate of the rejection level for models with nonevolving GRB source population is the ratio of the maximum NE likelihood factor (NE,Λ model in Table 2) to that for SF models (e.g., SF1,Λ in Table 2), which is $1.4 \cdot 10^{-4}$.

Figures 4, 5, and 6 demonstrate the differences between fits using NE and SF models. As seen in Figure 5, the high brightness slope of the $\log N - \log P$ distribution for the broken power law NE model is too flat and it cannot be made considerably steeper by modifying the LF. Note that the NE standard candle $\log N - \log P$ distribution with $I = 1 \text{ photon s}^{-1} \text{cm}^{-2}$ is already flatter than the observed $\log N - \log P$ distribution. Then if the LF is extended to $\sim 100 \text{ photons s}^{-1} \text{cm}^{-2}$, the model tail will be considerably flatter than the observed tail independently of how the LF is extended.

Looking at the integral distribution of real GRBs in Figure 6, one notices that it declines faster than an Euclidean distribution. However, this is still not a statistically significant fact. The probability of such a deviation from the $-3/2$ slope by chance is 0.1, which is relatively large (integral distributions are known to produce an illusion of statistically significant features from fluctuations). Most probably we are just dealing with a moderate fluctuation. Nevertheless, the observed slope could really be steeper than the Euclidean one if the decline of GRBs is steep enough. More data are required to clarify this issue.

The rejection of the NE models is significant even without the redshift data. The unconstrained rejection factor, taken as the ratio of the unconstrained likelihoods of the NE,Λ and SF1,Λ models is $\sim 2 \cdot 10^{-3}$ (see Table 2). This means that the result is not very sensitive to the value of the constraining N_{40} . If we, e.g., overestimate the rate of intrinsically strong GRBs by a factor 3 (suppose that it is a fluctuation) and that $N_{40} = 1$, then the rejection factor is $4 \cdot 10^{-4}$.

While the NE models are rejected using the low redshift behavior, one does not obtain any preference for a certain kind of SF evolution at large redshifts. Different SF models give similar likelihood results (see the Tables) except for the SF3 scenario, which gives a slightly worse fit. Furthermore, the data do not allow us to distinguish between matter-dominated and vacuum-dominated cosmologies.

5.2. The Shape of the Luminosity Function

Once the NE models have been rejected at a significant level, we now concentrate on the SF models, i.e., models with evolution of the GRB source population. There are two clear features of the LF that we see for all SF models: a near power law interval at the lower brightness range and a break or turnover towards the bright end of the distribution. Attempting to replace this construction of the LF by a log-normal LF gives a decrease

of the maximum likelihood by 2 orders of magnitude (see, e.g., the two SF1 models in Table 1).

If we study the χ^2 topography for the broken power law LF, we find a power law fragment at least 1.7 orders of magnitudes wide and there is no upper limit on its width. It can be arbitrarily extended to lower brightnesses (see Fig. 7). Indeed, one can see from Figure 7 that the χ^2 distribution reaches its asymptotics: by extending the LF further to lower brightnesses does not affect the model in the range of the data points.

On the other hand, the slope of this power law is surprisingly well constrained, especially for the SF1 model (Fig. 7), and it is slightly sensitive to the chosen SF behavior at large redshifts. The shape of the χ^2 minimum changes, however. Larger SF rates at high redshifts allow flatter slopes α (see Fig. 8). The $\chi^2 - \alpha$ plots for a matter-dominated cosmology, which are not shown, are very close to those shown in Figure 8. They are just slightly narrower and more symmetric.

A break or a turnover is necessary at a high significance level. Its removal increases χ^2 by $\Delta\chi^2 \sim 30$ for SF1 and $\Delta\chi^2 \sim 19 - 25$ for SF2 models (see Table 2). The properties of the break are, however, less certain than the parameters of the power law fragment. The χ^2 minimum is non-parabolic, asymmetric and relatively wide as seen in Figure 9. All we can say is that some turnover in the power law LF is required at an intrinsic brightness of about 10 photons $\text{s}^{-1} \text{cm}^{-2}$ at $z = 1$, or $\sim 3 \cdot 10^{51} \text{erg s}^{-1}$ for isotropic emission. The fitted position of the break is slightly sensitive to the cosmological model but the difference is within the statistical errors. We, however, can not distinguish between a power law break and an exponential cutoff of the LF. Both give a good χ^2 and the same maximum likelihood (compare Tables 1 and 2). Summarizing, we can claim that the behavior of the LF below $I \sim 3 \text{ photons s}^{-1} \text{cm}^{-2}$ or $10^{51} \text{erg s}^{-1}$ (in the 50 - 300 keV range) is close to the power law $dN/dI \propto I^{-1.5}$ (or, more exactly, the power law index $\alpha - 1$ can vary from ~ -1.35 to ~ -1.5 depending on the model). Then it breaks to a steeper slope. A smooth break (i.e., the parametrization SBPL in section 3.3) also gives a good result. The likelihood is 0.016 for the SF2, Λ model when the difference in the slopes is large enough, i.e., $\beta < -3$.

Figure 10 shows a set of the best fit LFs for different models. The reason why the best fit LFs are more or less well defined is clear when comparing the LF curves with the BATSE log N - log P distribution shown by the crosses. The latter should be a convolution of the former with the standard candle curves in Figure 2. For the SF1 and SF2 models, the standard candle curves are “narrower” than the BATSE log N - log P distribution. Therefore the LF should roughly correspond to the main features of the observed log N - log P distribution: a power law with a turnover. In the case of the SF1 model with narrower redshift distribution, the LF is closer to the observed brightness distribution (see Fig. 10). It is natural that the required turnover of the LF is sharper than that of the log N - log P distribution with the sharp LF turnover being smoothed by the convolution.

5.3. The lower limit on the total GRB rate

The last column of Table 2 shows the lower limits on the total rate of GRBs in the visible universe. These limits correspond to $\Delta\chi^2 = 7$, i.e., to 1σ of a χ^2 distribution with 25 DOF. Note that their values are obtained using an abrupt cutoff of the LF at the dim end. For the SF2, Λ model, the highest allowed cut off is at $\sim 0.4 \cdot 10^{50} \text{erg s}^{-1}$. A more realistic smoother cut off would give a higher lower limit. We suggest that the value 3000

GRBs per year gives a realistic estimate of the minimum GRB rate. This estimate is for *long* GRBs only. The result depends on the SF model in a natural way predicting a larger result for a higher SF rate at large redshifts.

For the SF2, Λ model of the GRB source evolution, the highest minimum comoving GRB rate at large redshifts is $\sim 3 \text{ yr}^{-1} \text{Gpc}^{-3}$. At the present epoch, it becomes $0.13 \text{ yr}^{-1} \text{Gpc}^{-3}$. This lower limit coincides with the value claimed by Porciani & Madau (2001) as the estimate derived from a fit of the data of Kommers et al. (2000). It is, however, very difficult to compare results as the slopes and the ranges of the LF are different. In fact, the shape of the LF derived by Porciani and Madau has the same parametrization as one of our models, a power law with an exponential cut off, but, nevertheless, contradict our results predicting a different slope and a finite estimate for the low brightness cutoff of the LF. The latter could be a consequence of the different behavior of the log N - log P distribution near the threshold in Kommers et al. (2000).

Our estimate is close to the result of Schmidt (2000) which is $\sim 0.2 \text{ yr}^{-1} \text{Gpc}^{-3}$ at $z = 0$ derived assuming that the present GRB rate is 10 times less than at $z \sim 1.5$ (in our case the decline is a factor 23). On the basis of this estimate, we can discuss the possible association of GRB980425 and the supernova SN 1998bw (Bloom et al., 1999, see also Lamb, 1999 for a discussion). Schmidt (2000) estimates the probability of events such as GRB980425 if the association is real as being as low as 10^{-3} yr^{-1} . Indeed, the distance to SN 1998bw is $\sim 40 \text{ Mpc}$. The corresponding sampling volume is $2.7 \cdot 10^{-5} \text{ Gpc}^3$. Our estimate of the GRBs rate $0.13 \text{ yr}^{-1} \text{Gpc}^{-3}$ with the cutoff $\sim 3 \cdot 10^{49} \text{erg s}^{-1}$. The 50 - 300 keV peak luminosity of GRB980425 is $3 \cdot 10^{46} \text{erg s}^{-1}$ (our rough estimate). If the luminosity function extends down to this luminosity with the determined slope $\alpha - 1 \approx -1.4$, then the rate of GRBs above this luminosity will be ~ 20 times larger, i.e., $2.6 \text{ yr}^{-1} \text{Gpc}^{-3}$ at $z = 0$ and a corresponding rate of $0.7 \cdot 10^{-4} \text{ yr}^{-1}$ in the sampling volume. Furthermore, one should take into account the probability that such events will be localized with the accuracy of a few arcseconds which reduces the estimate by at least an extra order of magnitude. Thus the probability of occurrence and good localization of an event such as GRB980425 within $\sim 40 \text{ Mpc}$ with the power law behavior of LF down to $10^{46} \text{erg s}^{-1}$ is below 10^{-5} per year. Such a small probability can hardly be compensated by a break in the LF below the observational cut off. The break must be so steep that it will affect the observed log N - log P distribution near the BATSE threshold. This is a strong argument that GRB980425 might represent a different phenomenon that does not overlap with classic GRBs in its luminosity function (but at the same time being indistinguishable from typical GRBs in its general appearance). A more probable possibility is that we are dealing with an accidental coincidence.

6. CONCLUSIONS

The source population of GRBs sharply declines from $z \sim 1.5$ towards the present epoch. This fact is established at the confidence level 10^{-4} . The measured decline of the star formation rate being used as the evolution hypothesis for the source population of GRBs fits the data satisfactorily.

This is what is expected according to prevailing view of GRBs as being the product of stellar evolution. Such a scenario was already successfully applied for the description of the observed log N - log P evolution, e.g., by Wijers et al. (1998), Panchenko (1999), Kommers et al. (2000), Schmidt (2000),

and Porciani & Madau (2001). However, nobody has quantitatively demonstrated that an evolution similar to the SF rate at some range of z is *necessary* to describe data. We can mention just the work of Schmidt (2000) where the SF rate hypothesis fits the bright tail of the $\log N - \log P$ distribution better (by a visual impression) than the NE hypothesis. However, no quantitative comparison of different scenarios has been done. We have here demonstrated that the decline of the GRB population consistent with the SF decline is a *necessary* requirement.

The main issue is whether the GRBs are associated with the collapse of massive stars (collapsars) or the merging of neutron stars (mergers). On the small scale, these scenarios differ regarding the expected correlations of GRBs with star formation regions in galaxies: collapsar GRBs should be well correlated, merger GRBs should show no correlation with the star formation. This fact stimulated searches for such correlations using optical GRB afterglows (see, e.g., the review of van Paradijs, Kouveliotou, & Wijers, 2000). On the cosmological scale, such correlations should exist in both cases. However, in the merger scenario the occurrence of GRBs will be described by the SF rate convolved with a delay function. If the latter extends to a few billions years, then the decline of the GRB population will be considerably flatter. For estimates of the delay function for mergers, see Portegies Zwart & Yungelson (1998) and Panchenko et al. (1999).

Qualitatively, our results favor the collapsar scenario. A very interesting situation occurs if the very steep, steeper than $-3/2$, slope of the $\log N - \log P$ tail as shown in Figure 5 will persist to larger P (*Ulysses* data reduced by Atteia, Boer & Hurley, 1999 indicate that this can be the case). Then one will have to accept that the GRB progenitors are very massive collapsars whose population can decline faster than the general SF rate.

But, at present, we do not have sufficient statistical arguments to rule out mergers. We believe that the data can give tight constraints on the delay function for the merger scenario and the latter can be challenged by such constraints. However, we leave such estimates for future studies for the reason that in order to obtain solid conclusions, it is worth to incorporate the *Ulysses* data, which would provide at least a doubling of the statistics of the brightest GRBs.

Our results concerning the luminosity function of GRBs confirm the conclusion of Loredo & Wasserman (1998) that the width of the luminosity function is not constrained by the BATSE data being wider than two orders of magnitude. The shape of the LF tried in the most of previous works was a truncated power law or a lognormal distribution which satisfied earlier data in a narrower brightness range. Schmidt (2000) used a broken power law hypothesis similar to one of our models. The position of the break is consistent with our results.

The interpretation of the shape of the luminosity function is beyond the scope of this work. In principle, such type of distributions - broken or exponentially cut power laws are common in nature. Then the break implies some physical limit such as a finite energy source. We believe that the outlined shape of the LF might be a useful clue in the development of physical models for the GRB emission.

This research made use of data obtained through the HEASARC Online Service provided by NASA/GSFC. This work was supported by the Swedish Natural Science Research Council, the Royal Swedish Academy of Science, the Wenner-Gren Foundation for Scientific Research, and the Russian Foundation for Basic Research grant 00-02-16135. We thank the anonymous referee for useful suggestions.

REFERENCES

Andersen, M. I., et al. 2000, A&A, 364, L54
 Atteia, J.-L., Boer, M., & Hurley, K. 2001, in Proc. of the 19th Texas Symposium on Relativistic Astrophysics and Cosmology, Ed. J. Paul, T. Montmerle, & E. Aubourg (CEA Saclay), 4
 Band, D., et al. 1993, ApJ, 413, 281
 Bloom, J. S., et al. 1999, Nature, 401, 453
 Bulik, T. 1999, in ASP Conf. Series 190, Gamma-Ray Bursts: The First Three Minutes, ed. J. Poutanen, & R. Svensson (San Francisco: ASP), 219 (astro-ph/9911437)
 Djorgovski, S. G., et al. 1999, GCN Circ. 251
 Fishman, G. J., et al. 1989, in Proc. of the Gamma Ray Observatory Science Workshop, ed. W. N. Johnson (Greenbelt: GSFC), 3
 Hakkila J. et al. 1996, ApJ, 462, 125
 Komers, J. M., Lewin, W. H. G., Kouveliotou, C., van Paradijs, J., Pendleton, G. N., Meegan, C. A., & Fishman, G. J. 2000, ApJ, 533, 696
 Krumholz, M., Thorsett, S. E., & Harrison, F. A. 1998, ApJ, 506, L81
 Lamb, D. Q. 1999, A&AS, 138, 607
 Ioyd, N. M. & Petrosian, V. 1999, ApJ, 511, 550
 Loredo, T. J., & Wasserman, I. M. 1998, ApJ, 502, 75
 Lukash, V. N. 2000 (astro-ph/0012012)
 Panchenko, I. 1999, in ASP Conf. Series 190, Gamma-Ray Bursts: The First Three Minutes, ed. J. Poutanen, & R. Svensson (San Francisco: ASP), 271 (astro-ph/9910450)
 Panchenko I. E., Lipunov V. M., Postnov K. A., & Prokhorov M. E. 1999, A&AS, 138, 517
 Porciani, C., & Madau, P. 2001, ApJ, 548, 522
 Portegies Zwart, S. F., & Yungelson, L. R. 1998, A&A, 332, 173
 Schmidt, M. 1999, A&AS, 138, 409
 Schmidt, M. 2000 (astro-ph/0001121)
 Stern, B. E., Tikhomirova, Ya., Stepanov, M., Kompaneets, D., Berezhnoy, A., & Svensson, R. 2000, ApJ, 540, L21
 Stern, B. E., Tikhomirova, Ya., Kompaneets, D., Svensson, R., & Poutanen, J. 2001, ApJ, 562, in press (astro-ph/0009447)
 Totani, T. 1999, ApJ, 511, 41
 van Paradijs, J., Kouveliotou, C., & Wijers R. A. M. J. 2000, ARA&A, 38, 379
 Wijers, R. A. M. J., Bloom, J. S., Bagla, J. S., & Natarajan, P. 1998, MNRAS, 294, L13
 Vreeswijk, P. M., et al. 1999, GCN Circ. 496

TABLE 1

BEST FITS OF DATA TO SOME COSMOLOGICAL MODELS WITH DIFFERENT FORMS OF THE LF.

Model	LF	χ^2	M_{50}	Likelihood	α	δ	ΔI_0
NE,Λ	TPL	36.8,39.8	11.5	$1.3 \cdot 10^{-4}$	$-0.37^{+0.27}_{-0.31}$		2.8, 10.7
NE,Λ	LGN	44.3,42.5	16.6	$1.2 \cdot 10^{-6}$		1.9	0.032, 0.36
NE,Λ	PLexp	54.0, 49.7	18.7	$2 \cdot 10^{-8}$	$-0.21^{+0.71}_{-0.38}$		15, 21
SF1,Λ	LGN	44.5,39.8	6.0	$3 \cdot 10^{-4}$		2.0	0.032, 0.12
SF1,Λ	PLexp	31.2,30.7	7.0	0.022	-0.43 ± 0.09		14, 28
SF2,Λ	PLexp	34.2,31.7	6.7	0.016	$-0.36^{+0.13}_{-0.10}$		11, 33
SF2,M	PLexp	32.7,31.4	6.9	0.018	$-0.36^{+0.10}_{-0.08}$		12, 26

Note. — For models and LF parametrizations, see §§3.1-3.3. The fit with the LF unconstrained by the redshift data is given only for TPL case. For all other given fits, the LF is constrained by $N_{40} > 3$ yr^{-1} . The χ^2 values are given at the maximum likelihood and the minimum χ^2 points, respectively. The "Likelihood" is the product of the χ^2 probability and the Poisson probability of sampling not more than 3 events at a given expected number M_{50} . M_{50} is given at maximum likelihood point. α is the slope of the power law part of the LF. δ is the width of the log-normal distribution (see §3.3). I_0 is the upper cut off brightness of the truncated power law LF, the center of the log-normal distribution, or the exponential cutoff energy for the PLexp LF (see §3.3). The errors in α and the confidence interval, ΔI_0 , for I_0 correspond to $\Delta \chi^2 = 4$ (corresponding to 2σ in the conventional interpretation. However, one should be careful with such an interpretation when the results depends on missing data points below the threshold).

TABLE 2

BEST FITS OF DATA TO ALL EVOLUTION MODELS WITH A BROKEN POWER LAW LF

Model	χ^2	M_{50}	Likelihood	Uncon. lk.	α	ΔI_0	$\Delta \chi^2$	$N_{\text{tot}} \text{ yr}^{-1}$
NE,M	39.1	16.8	$6 \cdot 10^{-7}$	$4 \cdot 10^{-5}$	-0.32 ± 0.50	0.23, 3.3	7.	2800
NE,Λ	40.4	14.5	$3.2 \cdot 10^{-6}$	$0.87 \cdot 10^{-4}$	$-0.3^{+1.}_{-0.4}$	0.43, 5.0	5.	3000
SF1,M	29.0	7.2	0.015	0.043	-0.49 ± 0.08	2.8, 9.2	33	1800
SF1,Λ	29.4	6.7	0.023	0.050	-0.48 ± 0.09	2.9, 16.	28	2000
SF2,M	30.2	6.8	0.018	0.031	-0.44 ± 0.11	2.9, 15.	25	2700
SF2,Λ	30.3	6.0	0.021	0.028	-0.43 ± 0.12	3.4, 21.	19	3000
SF3,M	30.9	7.2	0.014	0.20	-0.38 ± 0.12	2.9, 11.	21	4400
SF3,Λ	30.7	6.55	0.014	0.17	$-0.34^{+0.17}_{-0.14}$	4.2, 21.	16	4500

Note. — The LF is parametrized as a truncated broken power law with 4 free parameters (the BPL model in §3.3). The number of degrees of freedom is 25. Many details are given in the Note of Table 1. α is the slope of the power law part of the LF below the break. The errors correspond to a $\Delta \chi^2 = 4$ confidence interval. ΔI_0 is the confidence interval ($\Delta \chi^2 = 4$) of the break in the LF, I_0 , in photons $\text{s}^{-1} \text{cm}^{-2}$ at $z = 1$. Introducing a break in a single power law gives the χ^2 reduction, $\Delta \chi^2$, in the next column. N_{tot} is the lower limit of the total GRB rate per year.

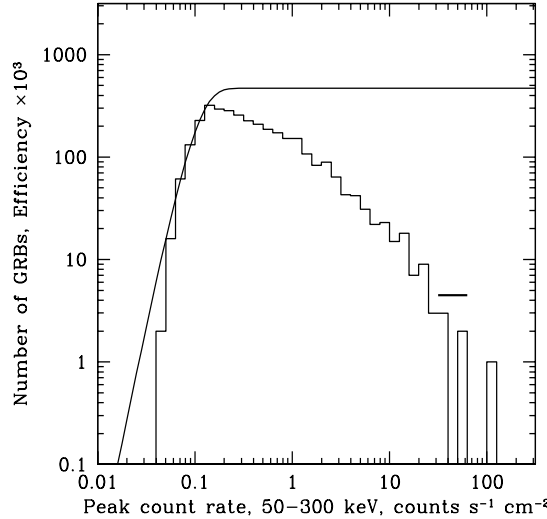


FIG. 1.— Fitted data. The histogram is the raw count rate distribution of the sample of 3255 long GRBs found in the continuous BATSE records. The solid curve is the efficiency function $E(c_e)$ in equation (1) measured using the test burst method. The discrepancy at the threshold results from the brightness bias (see eq. 1) and is removed using the efficiency matrix. The thick horizontal bar on the right tail of the distribution shows the count rate contribution of the three intrinsically brightest events with measured redshifts if they were emitting at $z=1$. The number of these events is renormalized to the 9.1 years of the BATSE observations. Their original number is 3 over ~ 2 years.

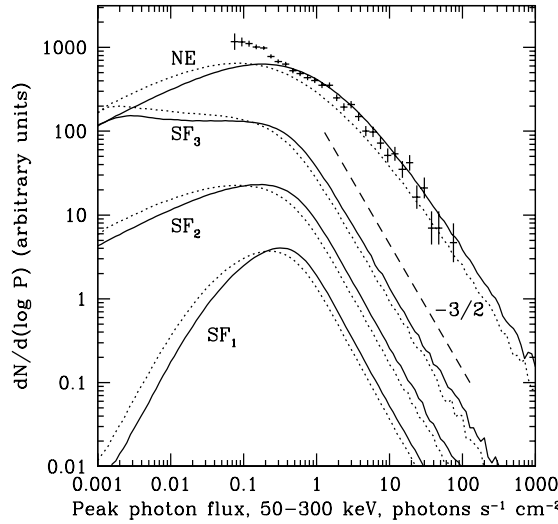


FIG. 2.— Standard candle log N - log P distributions for different models. The standard candle brightness corresponds to a photon peak flux of 1 photon $s^{-1} cm^{-2}$ at $z = 1$. From top to bottom: no evolution (NE), SF₃ (eq. 6), SF₂ (eq. 5), SF₁ (eq. 4). Solid curves - $(\Omega_M, \Omega_\Lambda) = (1, 0)$, dotted curves - $(\Omega_M, \Omega_\Lambda) = (0.3, 0.7)$. The crosses represent the observed log N - log P distribution of 3255 long BATSE GRBs.

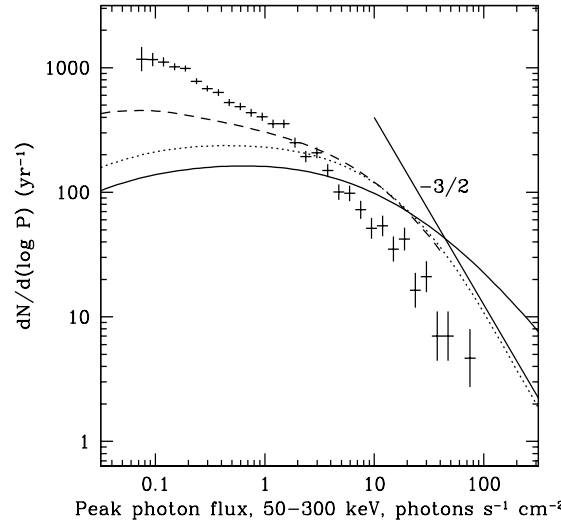


FIG. 3.— Test for the luminosity distribution inferred from the sample of 17 events with known redshifts and intrinsic luminosities. Log N - log P distributions obtained with the luminosity distribution of this sample are compared to the BATSE data (crosses) for different evolutionary models. Solid curve: NE model; dotted curve: SF2 model; dashed curve: SF3 model. The striking disagreement which can not be compensated with a reasonable redshift distribution shows that one can not rely on redshift data in the whole luminosity range because of a strong luminosity dependent selection bias. The used cosmology was $(\Omega_M, \Omega_\Lambda) = (0.3, 0.7)$.

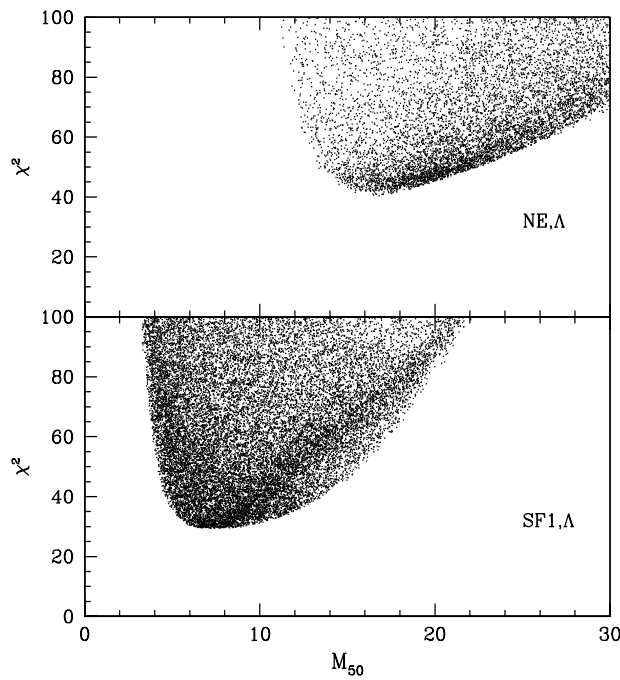


FIG. 4.— Fits of the bright tail of the log N - log P distribution using a broken power law LF. The value of χ^2 versus the predicted number of bright events M_{50} at $N_{40} > 3 \text{ yr}^{-1}$. Actual value of M_{50} is 3. Parameters I_1, I_0, α , and β are random. The models are NE, Λ (upper panel) and SF1, Λ (lower panel).

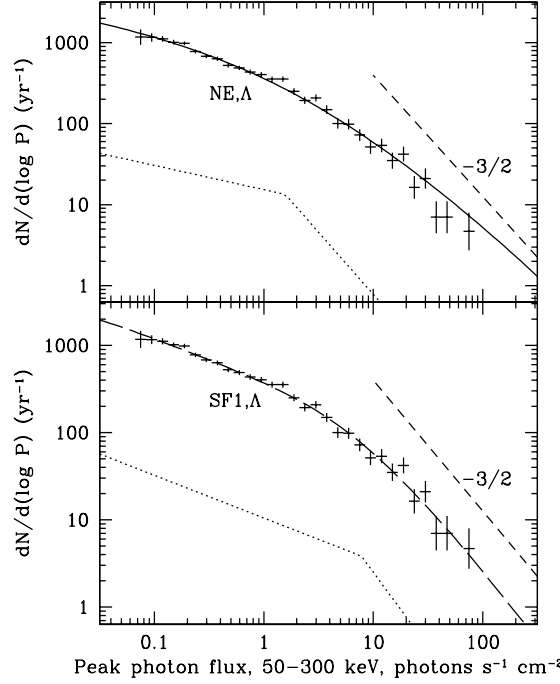


FIG. 5.— Best fits of data to models with no (upper panel, NE) and with SF1 (lower panel) GRB source evolution. Crosses are observed data points corrected using the efficiency matrix (1), solid curves - the models, dotted curves - the model LF (a broken power law), dashed line - the Euclidean $-3/2$ slope. The LF corresponds to a GRB luminosity distance at $z = 1$ with an arbitrary normalization of the rate. The cosmological model has $(\Omega_M, \Omega_\Lambda) = (0.3, 0.7)$. For fitting parameters, see Table 2.

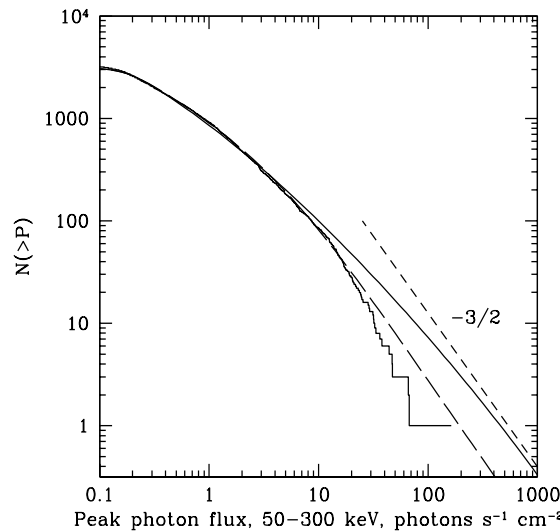


FIG. 6.— The same best fit functions as in Figure 5 but in integral form. Histogram - the raw peak count rate distribution in integral form ($N(> P)$) - the number of GRBs with peak flux larger than P), solid curve - the NE,Λ model, dotted curve - the SF1,Λ model, and dashed line - the Euclidean distribution. The model curves are convolved with the efficiency matrix to correspond to the raw data in this figure.

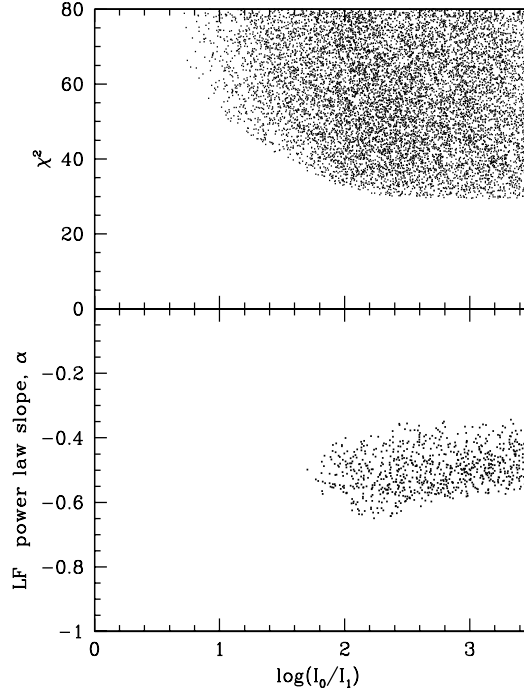


FIG. 7.— The confidence area for parameters of the power law fragment of the broken power law LF. The model is SF1, Λ . The confidence area corresponds to $\Delta\chi^2 < 6.17$, which formally corresponds to a 2σ confidence interval. However, see Notes of Table 1.

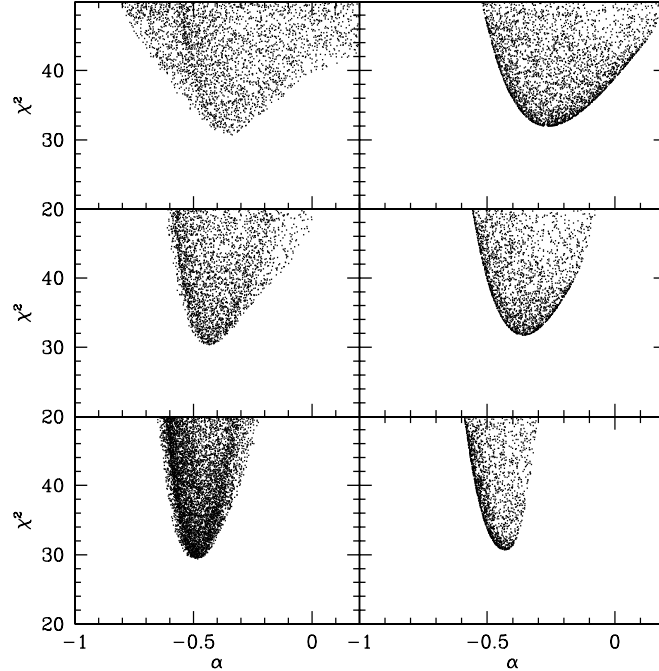


FIG. 8.— The profile of the χ^2 minima for the power law slope α . Left panels: for a broken power law LF; right panels: for the PExp LF. From bottom to top: the SF1, Λ , SF2, Λ , and SF3, Λ models.

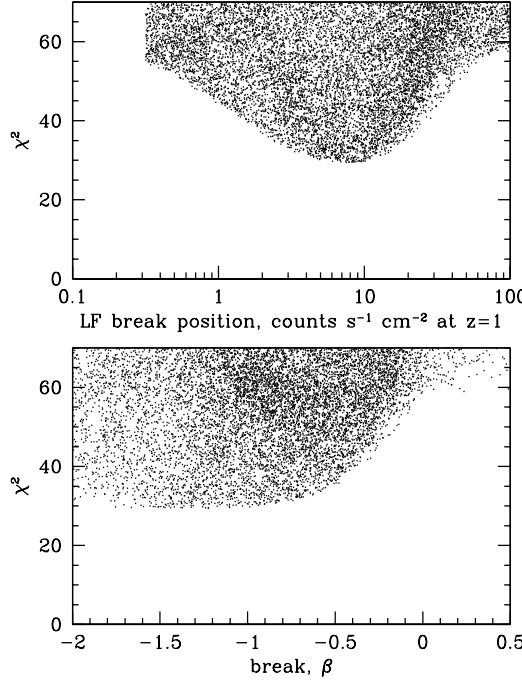


FIG. 9.— The characteristics of the power law break in the broken power law LF for the SF1, Λ model. Upper panel: χ^2 versus the position of the break, I_0 , in the intrinsic peak brightness scale. Lower panel: χ^2 versus the power law slope difference. Other parameters are random.

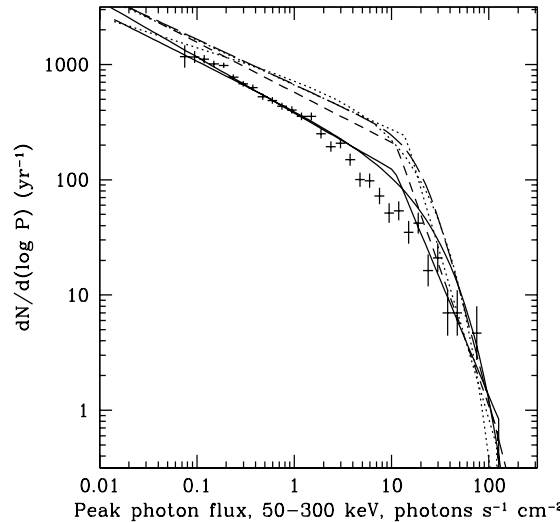


FIG. 10.— Best fit luminosity functions for different models. Dotted curves: a broken power law and the PLexp for the SF2, Λ model; dashed curve: the broken power law for the SF2, M model; dash-dotted curve: the smoothly broken power law (SBPL, see section 3.3) for the SF2, Λ model; solid curves: a broken power law and the PLexp for the SF1, Λ model. The normalisation of the intrinsic brightness scale corresponds to the peak photon flux being emitted at $z = 1$. Crosses show real data points versus the *apparent* brightness, where the distance for each event is unknown. Thus the ordinate for real data has a different meaning.